The effect of two types of C-S-H on the elasticity of cement-based materials: Results from nanoindentation and micromechanical modeling

Georgios Constantinides, Franz-Josef Ulm

The effect of two types of C-S-H on the elasticity of cement-based materials: Results from nanoindentation and micromechanical modeling

Georgios Constantinides, Franz-Josef Ulm

Department of Civil and Environmental Engineering, Massachusetts Institute of Technology, 77 Massachusetts Avenue, Cambridge, MA 02139-4307, USA

It has long been recognized, in cement chemistry, that two types of calcium-silicate-hydrate (C-S-H) exist in cement-based materials, but less is known about how the two types of C-S-H affect the mechanical properties. By means of nanoindentation tests on nondegraded and calcium leached cement paste, the paper confirms the existence of two types of C-S-H, and investigates the distinct role played by the two phases on the elastic properties of cement-based materials. It is found that (1) high-density C-S-H are mechanically less affected by calcium leaching than low density C-S-H, and (2) the volume fractions occupied by the two phases in the C-S-H matrix are not affected by calcium leaching. The nanoindentation results also provide quantitative evidence, suggesting that the elastic properties of the C-S-H phase are intrinsic material properties that do not depend on mix proportions of cement-based materials. The material properties and volume fractions are used in a novel two-step homogenization model, that predicts the macroscopic elastic properties of cement pastes with high accuracy. Combined with advanced physical chemistry models that allow, for a given w/c ratio, determination of the volume fractions of the two types of C-S-H, the model can be applied to any cement paste, with or without Portlandite, Clinker, and so on. In particular, from an application of the model to decalcified cement pastes, it is shown that that the decalcification of the C-S-H phase is the primary source of the macroscopic elastic modulus degradation, that dominates over the effect of the dissolution of Portlandite in cement-based material systems.

Keywords: Nanoindentation; Elastic moduli; Micromechanics; Calcium-silicate-hydrate (C-S-H); Microstructure

1. Introduction

It is now well established that calcium-silicate-hydrates (C-S-H) in cement-based materials exist in, at least, two different forms. First observations can be traced back to Taplin [1], who attributed the two families to the inner and outer hydration products. Early indicative studies employed light microscopy of thin sections [2], which were later confirmed by means of high-resolution TEM of ground and redispersed material [2–6], X-ray mapping of flat polished sections [6–8], Neutron Scattering [9] and other techniques. These studies provide clear evidence of the existence of two morphological entities of C-S-H. More recently, based on a comprehensive analysis of disparate measurements of specific surface area of hardened cement pastes (hcp) reported in the open literature, Jennings [10] and Tennis and Jennings [11] proposed a model for the two types of C-S-H, with distinct volume fractions and geometry. The two types of C-S-H have been referred to, in the open literature, as the C-S-H portions of phenograins–groundmass [12], outer product–inner product [1], low density–high density [10,11], or middle product–late product [13,14]. Table 1 summarizes the different classifications of the two types of C-S-H.

While the existence of two types of C-S-H appears as a well-established fact in cement chemistry (see Table 1), little is known about the mechanical contribution of the C-S-H types on the macroscopic material properties of cement-based materials. These are the focuses of this paper: (1) to investigate experimentally the elastic performance of cement paste at different length scales, in particular at levels where the individual chemical constituents can be identified, complementing physical chemistry investigations on the mechanics side; and (2) to upscale this contribution from the microlevel to the macrolevel of cement-based materials by means of advanced homogenization models.

E-mail address: ulm@mit.edu (F.-J. Ulm).
URL: http://cist.mit.edu.

Table 1
Classification of the two morphological entities of C-S-H as found in the open literature

Classification	Reference
Inner Product–Outer Product	Taplin [1], Richardson [6], Groves [3]
Middle Product–Late Product	Scrivener et al. [13], Taylor [14]
Phenograins–Groundmass	Diamond and Bonen [12]
Low Density–High Density	Jennings [10], Tennis and Jennings [11]

The combined experimental–theoretical investigation is carried out on two reference states of an ordinary Portland cement paste (w/c = 0.5): a nondegraded hcp in its initial state, and a chemically degraded hcp obtained by accelerated calcium leaching. The employed leaching process dissolves the Portlandite crystals [$CH = Ca(OH)_2$] and partially decalcifies the C-S-H of the cement paste. The rational behind the employment of calcium-leached materials in our study is that the two reference states (nondegraded vs. degraded) may be considered as asymptotic physical states of cement-based materials, particularly of the one employed in concrete structures exposed to a wetting agent (i.e., in dams, tunnels, pipes, nuclear containments, etc.). The mechanical effects of calcium leaching on cementitious materials has been investigated by several researchers with emphasis placed on the degradation of strength properties [15–22]. The degradation of elasticity, however, has not been investigated to the same extent, and studies are mainly restricted to macroscopic (10^{-2} m) measurements of the elasticity modulus by uniaxial compression tests and three-point bending tests within the framework of damage mechanics [16–18,23], or chemo-mechanics [21]. On the other hand, little is known about the effect of calcium leaching on the intrinsic elastic properties of the individual cement paste constituents and especially on the properties of the two types of C-S-H. Therefore, by providing a comprehensive understanding of the mechanical role played by the two types of C-S-H in the two asymptotic states (nondegraded vs. degraded) and at different scales, the approach developed in this paper is expected to close this knowledge gap, and is intended to serve as a basis for prediction of the long-term behavior of aging materials in concrete structures.

For reference, the multiscale approach developed in this paper considers four elementary levels of the microstructure of concrete (see Fig. 1):

1. The presence of the two types of C-S-H is estimated at a scale of 10^{-6}–10^{-8} m (Level I), which is the smallest material length scale that is, at present, accessible by mechanical testing. In this paper, the elastic properties of the individual constituents are assessed by nanoindentation tests (10^{-7}–10^{-4} m), while complementary scanning electron microscope investigation (SEM) pro-

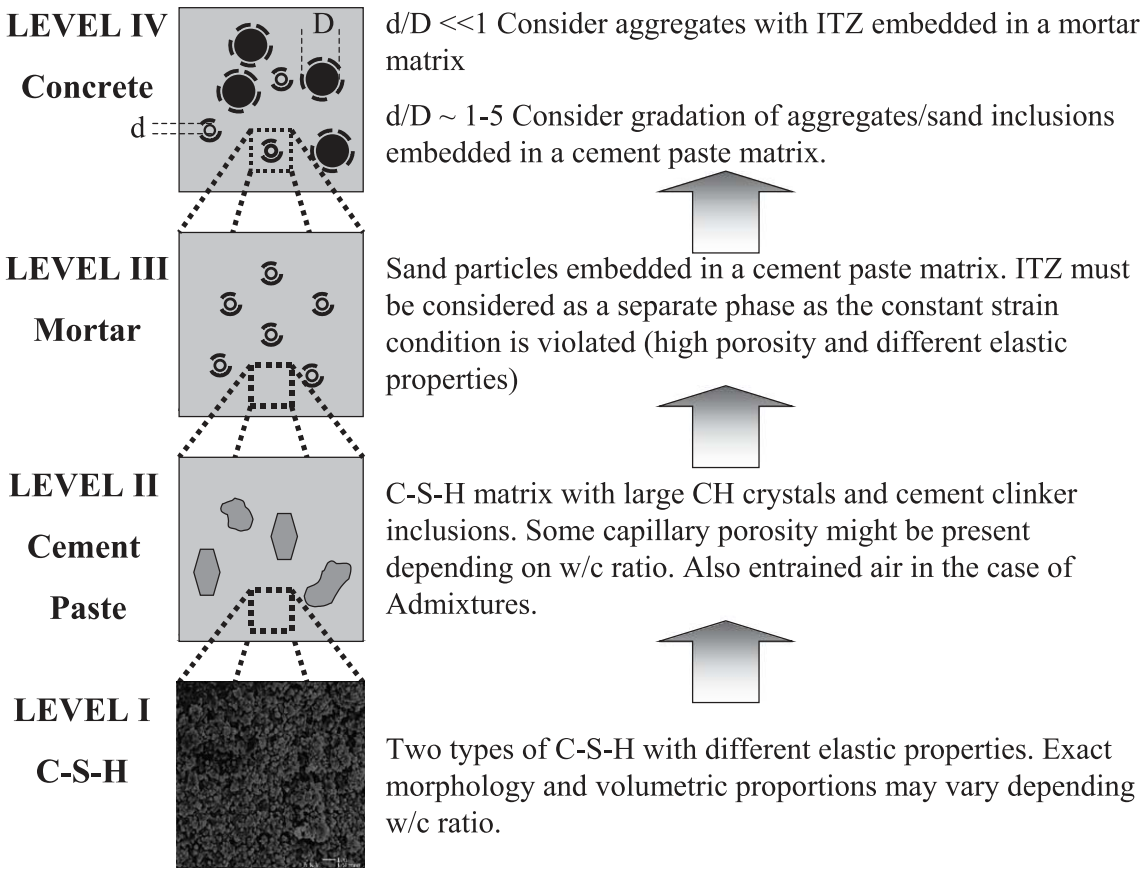

Fig. 1. Four-level microstructure of cement-based composite materials.

vides additional qualitative information about the microstructure and its evolution through calcium leaching. It is also the starting point for the homogenization approach developed in this paper.
2. The C-S-H matrix together with large CH crystals, cement clinker and micrometer porosity in the case of high w/c ratios forms the cement paste, and is referred to as Level II (10^{-4}–10^{-3} m). The elastic properties of nondegraded and degraded cement paste are assessed in this study by ultrasonic pulse velocity (UPV) tests.
3. Level III (10^{-3}–10^{-1} m) refers to mortar; that is a three phase composite material composed of a cement paste matrix, sand particle inclusions, and an interfacial transition zone (ITZ). This scale has been the focus of micromechanical modeling attempts, both analytically [24,25] and numerically [26,27]. Since the chemical attack occurs primarily at a much lower scale (Level I or II), these models, however, do not allow capturing the effect of chemical degradation on the effective macroscopic elastic properties.
4. Concrete as a homogeneous material is considered on Level IV (10^{-1}–10^{1} m), which is the scale of concrete engineering applications. Similar to Level III, homogenization approaches that consider at this scale a three-phase material composed of aggregates embedded in a mortar matrix and an ITZ have been developed [24–31].

The focus of the combined experimental–theoretical study developed below is Level I and II.

2. Experimental program

2.1. Materials and sample preparation

Cement paste was prepared at a water–cement ratio w/c = 0.5 using an ordinary Type I Portland cement. The composition of the cement is given in Table 2. The samples were cast in cylindrical molds of diameter 11.5 mm and length 60 mm. After 24 h, the specimens were demolded and cured in a saturated lime solution for 27 days at 20 °C. After curing, half of the samples were placed in a 6 mol/l ammonium nitrate solution for calcium leaching. In this accelerated leaching test, described in detail in Ref. [19], 'natural' leaching by pure water is accelerated by a factor of 300, with a Portlandite dissolution front that reaches the center of the 11.5 mm diameter samples after 9 days. The partial dissolution of the calcium in the C-S-H requires 45 days, at which complete and uniform calcium leached samples are obtained. At an age of 5 months, specimens from both batches were tested and compared. Specimens were kept in water at all times to avoid microcracking development.

Table 2
Type I Portland cement constituants, in mass percent

OPC type I					
CaO	SiO_2	Al_2O_3	MgO	SO_3	Na_2O
62.3	20.8	4.4	3.8	2.9	0.39
Fe_2O_3	K_2O	C_3Al	C_3S	C_2S	Ignition loss
2.4	1.28	8	53	20	0.66

Data provided by cement producer.

2.2. SEM investigation (Level I)

SEM investigation was carried out using a JEOL6320FV SEM of the Center of Materials Science and Engineering (CSME) at MIT. Cylindrical specimens were prepared with polished, epoxy-impregnated surfaces [32]. The finest polishing step was 0.25 μm. Samples were coated with Au-Pd before examination under the SEM. Working distance was around 19 mm, and low voltages (1–5 kV) were used to avoid charging.

Figs. 2 and 3 show SEM images of nondegraded and degraded cement paste at different resolutions. SEM images at a scale of 10^{-5}–10^{-4} m (Fig. 2) show that calcium depleted cement paste has a new class of pores, which is not present in the nondegraded material. This pore space can be attributed to the space previously occupied by large CH crystals. In addition, at a scale of 10^{-6} m (Fig. 3), a transformation of the C-S-H matrix phase due to calcium leaching can be seen. The small C-S-H subparticles in the nondegraded state form larger elementary units in the degraded state, that appear more continuous and more uniform, and that are perforated by micrometer sized pores. This change in microstructure of the C-S-H phase may be attributed to the reduction of the C/S ratio with decalcification. In fact, a decrease of the C/S ratio favors polymerization of the C-S-H chains [14, p. 118], [33] resulting in a material with continuous structure and larger subparticles. Similar observations have been reported for calcium leached materials using nuclear magnetic resonance (NMR) technique [34].

2.3. Nanoindentation (Level I)

Nanoindentation was carried out using a NanoTest 200 of the Laboratory of EXperimental and COMputational Micromechanics (LEXCOM) in the Department of Materials Science and Engineering at MIT. Cylindrical specimens were cut in slices 10–15 mm thick. The surfaces were ground and polished with silicon carbide papers and diamond particles to obtain a very flat and smooth surface finish. This was done in six stages of decreasing fineness with the last one being in the range of 0.25 μm. After polishing, the samples were placed in an ultrasonic bath to remove the dust and diamond particles left on the surface or in the porous structure.

2.3.1. The LEXCOM instrumented indentation

The employed nanoindenter allows monitoring the load (P)–displacement (h) relationship in a load range of 0 to 20 N, and in a displacement range of 0 to 50 mm, with

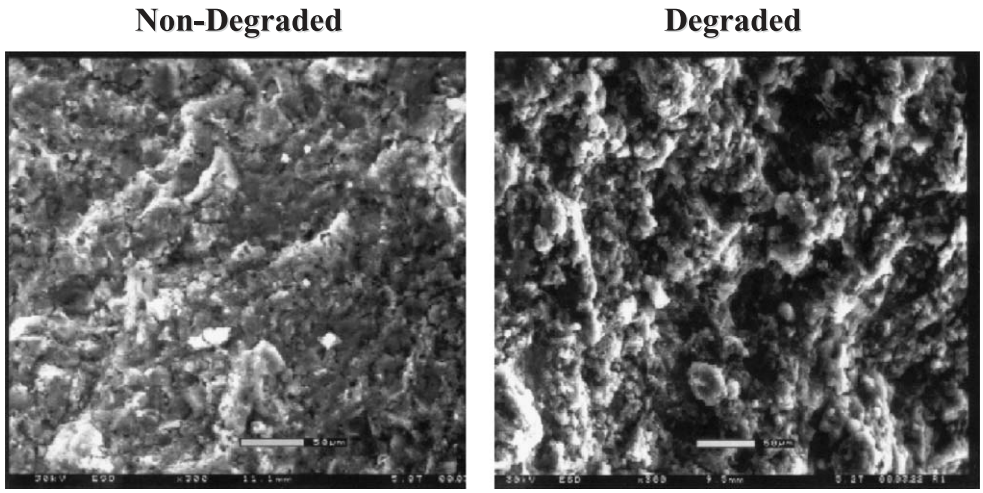

Fig. 2. Nondegraded (left) and degraded (right) cement paste seen at a 10^{-5} m scale. The new pore group created at that scale from the depletion of large CH crystals can be identified.

resolutions of 100 nN and 0.04 nm, respectively. In the test, described in detail in Refs. [35,36], a pendulum pivoting around frictionless bearings applies the load to the specimen. A current passes through a coil mounted at the top of the pendulum and attracts the coil to a fixed magnet. This sets the indenter into motion to the specimen surface which is firmly clamped to the loading stage. The displacement of the indenter (depth h of penetration into the specimen) is continuously monitored and recorded by the change in the capacitance of a parallel plate capacitor. In this way the complete $P-h$ response is obtained. A Berkovich indenter is employed in this study, and the loading rate used was 2.3 mN/s. The distance between indentation points was chosen in a way to avoid overlapping. Repeated loading–unloading cycles were performed in some of the tests to assess the pure elastic behavior of the material in that range.

Determination of the elastic recovery by analyzing the unloading data according to a model for the elastic contact problem leads to a solution for calculation of the elastic modulus E of the test area. Several methods have been proposed for analyzing the data. The most frequently used are the ones of Oliver and Pharr [37], Doerner and Nix [38] and the one developed at LEXCOM [35,39]. All three types of analysis were employed in this study. The results obtained with the LEXCOM and Oliver–Pharr models were in very good agreement (S.D. $< \pm 1\%$). Estimations of the elastic modulus using Derner and Nix method deviated by $\pm 10\%$. The data reported below are based on the LEXCOM method [40]. This method circumvents, by design, the need for visual observations of the contact area and incorporates into the analysis the effects of pile-up and sink-in.[1] This method gives access to the elasticity of a material domain defined by the diameter of the indenter impression provided it spans at least five times the characteristic length scale of the inhomogeneity at a scale below.

2.3.2. Results (Level I)

In our study, the characteristic length of the indentation area was on the order of 10^{-6} m (see Fig. 3), and the indentation depth varied in the range of 300–500 nm. Large Portlandite crystals were easily identified under the microscope, and their modulus was determined by indenting on them. However, measurements on the C-S-H could not be resolved with the use of the microscope due to their very small characteristic length, which is considerably smaller than the impression diameter. The nanoindentation results, therefore, appear to be characteristic of the C-S-H matrix phase, that is of the two types of C-S-H including C-S-H porosity. A series of 200 indentations covering an area of 1000 μm^2 (10 times the indentation area displayed in Fig. 3) was conducted on each specimen. The area was chosen to be statistically representative of the C-S-H matrix. The large amount of data lends itself to a statistical analysis. A frequency histogram of the elastic modulus obtained from nanoindentation is given in Fig. 4, from which the mean value and the standard deviation are extracted (see Table 3). We note:

1. The frequency distribution of the elastic modulus of the C-S-H matrix shows a clear bimodal structure, particularly in the degraded state (Fig. 4b). This bimodal distribution appears to be a mechanical expression of the existence of two types of C-S-H compounds present at a scale of 10^{-6}–10^{-7} m: a low stiffness C-S-H phase (C-S-H_a) and a high stiffness C-S-H phase (C-S-H_b). The middle peak in the nondegraded state can be attributed to the overlap of the two distributions due to the closeness of the stiffness of the two types of C-S-H compounds. If

[1] Quantification of these effects has been performed using 3-D finite element simulations of von-mises-type materials. Cement paste is believed to have a frictional behavior; should additional accuracy of the elastic modulus calculation is required, then the effect of the frictional behavior of the material to the contact area evolution should be taken into account.

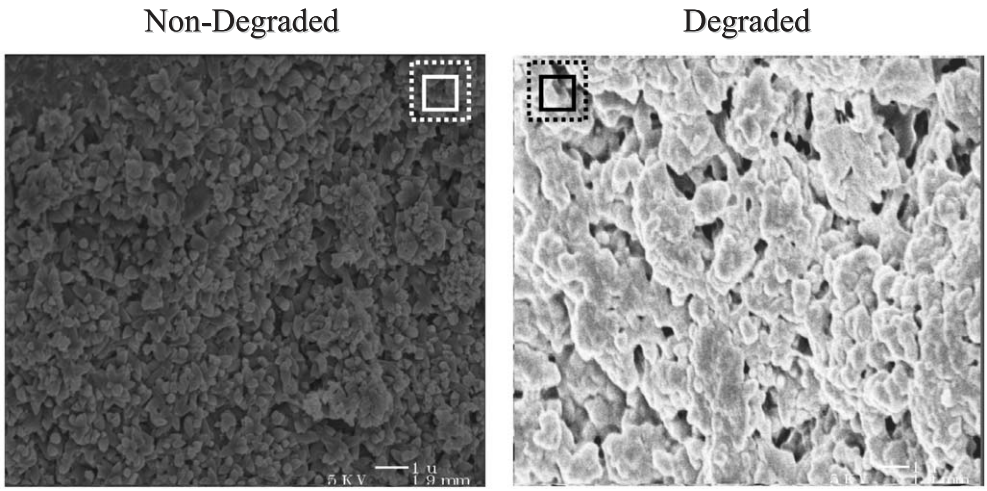

Fig. 3. SEM pictures of the C-S-H phase illustrating the transformation of the phase by chemical degradation; nondegraded (left), degraded (right). Solid and dotted squares in the picture indicate the approximate contact area and affected area during a single indentation.

we assume that the two types of C-S-H have identical elementary components at a scale below, it is reasonable to associate the low stiffness C-S-H with the outer product, i.e., low density C-S-H (C-S-H_a); and the high stiffness C-S-H with the inner product, i.e., high density C-S-H (C-S-H_b).

2. The mean values of the elastic modulus for the nondegraded material almost coincide with indentation data reported by Acker [41] on *Ductal*, an ultra high performance concrete produced at a very low w/c ratio (w/c = 0.18), and with admixtures. This suggests that the properties obtained by nanoindentation are intrinsic to all types of cement-based materials, and do not depend on the water–cement ratio, admixtures, etc. Additional tests are required to conclude on these evidence. The very existence of intrinsic properties at that scale could be

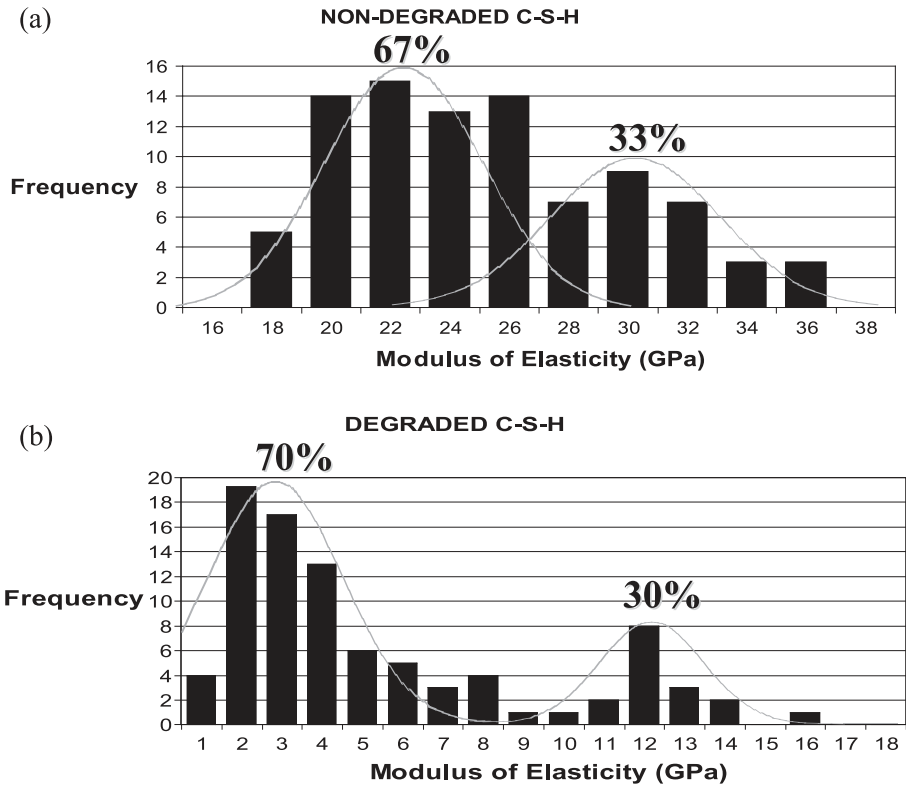

Fig. 4. Results obtained from nanoindentation. Elastic modulus frequency histogram for C-S-H in (a) nondegraded and (b) degraded state. Two types of C-S-H are identified; C-S-H_a and C-S-H_b. % indicates volumetric proportions obtained by measuring the area under the curves.

Table 3
Elastic modulus of individual constituents obtained by nanoindentation (Mean ± S.D.)

	Elastic modulus (GPa)		Residual value (%)
	Nondegraded	Degraded	
CH	38.0 ± 5	–	–
C-S-H_a	21.7 ± 2.2	3.0 ± 0.8	14
C-S-H_b	29.4 ± 2.4	12.0 ± 1.2	41

attributed to a characteristic packing or arrangement of the two C-S-H types during hydration.

3. Due to calcium leaching, both C-S-H phases exhibit a considerable loss of elastic stiffness. It is instructive to note from Fig. 4 that the low stiffness C-S-H_a is more heavily affected by the chemical degradation than the high stiffness C-S-H_b. The first has residual values of elastic modulus on the order of 14% of the initial one, in comparison to 41% for C-S-H_b (see Table 3). This observation can be attributed to the increase in porosity (< 1 μm), which gives rise to a higher surface area, and therefore to a higher level of exposure to severe degradation of the C-S-H_a phase. By contrast, enclosed C-S-H_b are less affected by the degradation.
4. Remarkably, the volumetric proportions of the two types of C-S-H that can be associated with the area under the curves in Fig. 4 are not affected by the degradation process. For the considered cement paste, the volume fraction of low stiffness C-S-H_a vs. high stiffness C-S-H_b is on the order of 70% vs. 30%, and these volume fractions remain approximately constant when moving from the nondegraded to the degraded state.

In summary, nanoindentation results support the existence of two families of C-S-H which maintain their volumetric proportions with calcium leaching. The loss of C-S-H stiffness can therefore be attributed to the decalcification of the two types of C-S-H (loss of their intrinsic elasticity) and/or to the increase of microporosity by leaching of probably engulfed nanocrystalline Portlandite and/or Ettringite (< 1 μm). Beaudoin and Feldman [42] provided experimental data of the mechanical properties of C-S-H with different C/S ratios suggesting that the intrinsic elastic properties of C-S-H are independent of the C/S ratio. This result, if verified, would indeed suggest that the decrease in C-S-H properties as measured by nanoindentation tests, results from an increase in porosity at lower scales.

2.4. Macroscopic measurements (Level II)

Macroscopic elasticity measurements on cement paste (Level II) were performed using high precision equipment (Fig. 5) of the Non-Destructive Evaluation Laboratory in the Department of Civil and Environmental Engineering at MIT. ASTM C 597-83 (Reapproved 1991) [43] and BS 1881: Part203 [44] provide a detailed description of the UPV technique. This long established nondestructive method determines the velocity of longitudinal (compressional) waves in a medium by measuring the time taken by the wave to travel a certain distance.

2.4.1. UPV measurements

The experimental set-up is illustrated in Fig. 6. The apparatus generates a pulse of vibration at an ultrasonic frequency, which is transmitted by an electroacoustic transducer (T) to the specimen through a water medium. Since the fluid does (almost) not transmit shear, only longitudinal waves are transferred to the specimen. Nevertheless, there are always some shear and surface waves, which however do not cause much interference, because the longitudinal waves travel at a much faster speed. Consequently, the exact

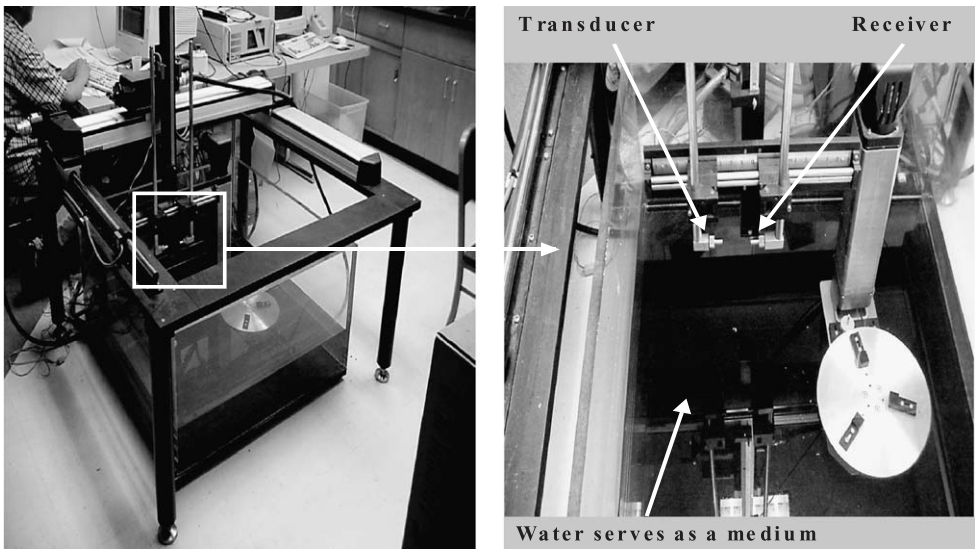

Fig. 5. Apparatus used for UPV measurements.

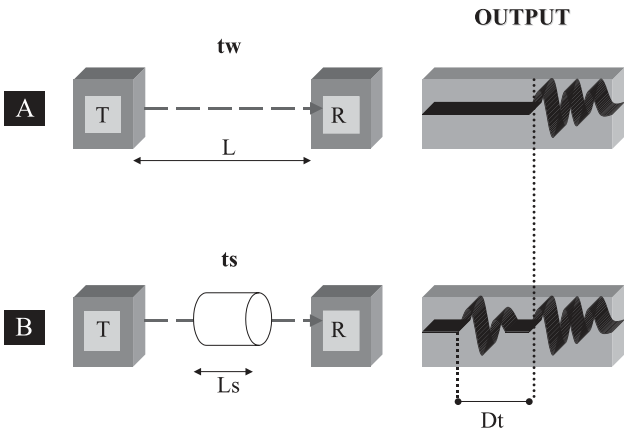

Fig. 6. UPV tests: Two types of measurements are required to calculate the velocity of ultrasound through the cementitious specimen.

time of arrival of the longitudinal wave can be picked up easily. After passing through the specimen, the vibrations are received and converted to an electrical signal by a second electroacoustic transducer which serves as a receiver (R). Once the signal is fed through an amplifier to a cathode-ray oscilloscope, the time of the pulse to travel the distance between the two transducers is measured with an accuracy of ± 0.01 μs. The water medium limits the error introduced by imperfect transducer–specimen contact. The presence of water medium, however, requires two experimental set-ups and measurements (Fig. 6) to isolate the velocity of sound through cement paste. In setup A, the time taken for the wave to travel through water (t_w) at a distance L [distance between transducer (T) and receiver (R)] is measured and the velocity of wave through water (C_w) is obtained from:

$$t_w = \frac{L}{C_w} \tag{1}$$

C_w was found to be equal to 1480 m/s at a temperature of 25 °C. In setup B, the specimen of length L_s is introduced in the travel path of the wave, and the time t_s taken for the wave to travel (through the sample and water) is now:

$$t_s = \frac{L - L_s}{C_w} + \frac{L_s}{C_L} = t_w - \frac{L_s}{C_w} + \frac{L_s}{C_L} \tag{2}$$

where C_L = velocity of wave through the specimen. The time taken for the wave to travel through the sample is $\Delta t = t_s - t_w$. Then, using Eq. (1) in Eq. (2), we obtain:

$$C_L = \frac{L_s C_w}{L_s - \Delta t \times C_w} \tag{3}$$

Eq. (3) gives access to the velocity of the pulse C_L in the concrete specimen by measuring the time delay Δt caused by the introduction of the concrete specimen in the line of pulse traveling. This time delay, Δt, is recorded by measuring the time shift between the two waves obtained in the two experimental set-ups (Fig. 6). Finally, with the knowledge of the length of the specimen, the density of the specimen ρ, and assuming a value for the Poisson's ratio v, the elastic modulus is obtained from:

$$E = \frac{C_L^2 \rho (1+v)(1-2v)}{(1-v)} \tag{4}$$

Relation (4) is restricted to linear, isotropic, homogeneous, and perfectly elastic materials. However, it can equally be applied to heterogeneous systems such as concrete when the dimension of the specimen (e.g., length $\mathcal{L}$) is large compared to the wave length λ [45]. Similarly, the wave length must be considerably larger than the size d of the elementary constituents of the material (characteristic dimension of heterogeneity):

$$d \ll \lambda \ll \mathcal{L} \tag{5}$$

In our study, applied frequencies varied in the range of 0.1–5 MHz giving approximate wave lengths on the order of $\lambda = 300$–900 μm. These wave lengths are large enough not to detect the elementary heterogeneities of the material; and they are small enough to avoid any surface interaction. These wave lengths satisfy the principle of separation of scales, expressed by Eq. (5), thus ensuring the good quality of the experiments. This method requires knowledge of the density and Poisson's ratio of the material. Density measurements were performed on all specimens and the corresponding values from Table 4 are used. Density values were calculated using volume and mass measurements. Length and weight measurements were performed with an accuracy of 0.01 mm and 0.001 g, respectively. In turn, values for Poisson's ratio were taken from the open literature. Results presented in [46] suggest that the macroscopic Poisson's ratio remains unaffected by the degradation process. In this study, a constant value of $v = 0.24$ was applied. A sensitivity analysis of the experimental results to a variety of parameters such as Poisson's ratio, wave length, frequency, support conditions, specimen size, and so on, can be found in Ref. [47].

2.4.2. Results (Level II)

The macroscopic results are summarized in Table 4. The macroscopic elastic modulus of calcium leached cement paste is significantly affected by chemical degradation with

Table 4
Macroscopic measurements: porosity (accessible to water), density and elastic modulus (Mean ± S.D.)

	Cement paste		Residual value (%)
	Nondegraded	Degraded	
Porosity (%)	39.7 ± 1.1	63.2 ± 1.6	163
Density (kg/m^3)	1898 ± 9	1351 ± 12	71
Elastic modulus (GPa)	22.8 ± 0.5	3.6 ± 0.2	16

The elastic modulus was determined using UPV measurements.

a residual value of 16%. This drop in macroscopic elasticity appears as a coupled consequence of (1) the increase in porosity due to the depletion of large Portlandite crystals; and (2) the loss of stiffness due to the decalcification of the C-S-H phase. A simple composite model following e.g., mixture theory cannot capture these different sources of chemical damage.

3. A two-step homogenization model for cement paste materials

The aim of the micromechanics model developed below is to upscale the intrinsic properties of cement paste from the micro- to the macrolevel. The backbone of the model is the four-level microstructure of concrete shown in Fig. 1. The four levels satisfy the separation of scale principle, that is, each level is separated from the next one by (at least) one order of magnitude in size of the elementary heterogeneity. This is a prerequisite for the application of upscaling schemes of continuum micromechanics [48]. Furthermore, from a morphological point of view, all levels are characterized by a matrix-inclusion geometry that can be effectively treated with the Mori–Tanaka scheme [49]. The Mori–Tanaka scheme is selected for its simplicity, and its very good performance in the characteristic concentration range of the multiple phases involved (typically, 10–30%), but also for the range of Poisson's ratios considered ($0.2 \le \nu \le 0.31$) [50].

3.1. Micromechanical representation

The contributions of the different constituents to the macroscopic stiffness of hardened cement paste take place at different observation scales. In particular, the two levels that separate the C-S-H phases at Level I from the cement paste at Level II, suggests a two-step homogenization procedure, as sketched in Fig. 7:

1. The first step consists in application of an appropriate homogenization scheme to Level I ($\mathscr{L} = 5-10$ μm). The nanoindentation results presented above provide clear evidence of two types of C-S-H, with different elastic properties that affect the overall elasticity of the composite. The average elastic properties determined by nanoindentation (see Table 3 and Fig. 4), however, include the effect of porosity and of any nanocrystalline CH or minor compounds present at smaller scales (<1 μm). The two types of C-S-H represent phases. A phase, in a micromechanical sense, is not necessarily a distinct material, but rather a subdomain of the overall matter characterized by an on-average constant stress or strain state. As such, a phase may well be composed of different materials. In this sense, the representative elementary volume (REV of volume V_p), displayed in Fig. 7a, is composed of two phases: a low density C-S-H$_a$ phase, and a high density C-S-H$_b$ phase, of volume fractions:

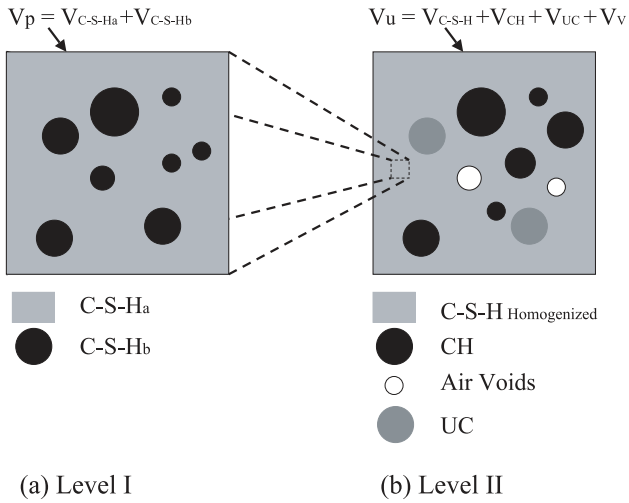

Fig. 7. Choice of REV for the two-step homogenization model for cement paste: (a) Level I; (b) Level II.

$$f_a = \frac{V_a}{V_p}; \quad f_b = \frac{V_b}{V_p}; \quad f_a + f_b = 1 \tag{6}$$

V_a and V_b are the volumes occupied by the two C-S-H phases. The volume fractions of the two C-S-H phases at this scale depend primarily on the w/c ratio, and are not affected by calcium leaching; that is for w/c = 0.5, from Fig. 4, $f_a = 0.7$; $f_b = 0.3$. Furthermore, from a morphological standpoint, the difference in stiffness of the two phases found by nanoindentation suggests that the stiffer C-S-H$_b$ phase plays the role of an inclusion phase embedded into a softer C-S-H$_a$ matrix. There are several micromechanics schemes suitable for this matrix inclusion morphology: dilute scheme, composite sphere model, three-phase model, Mori–Tanaka scheme, and so on. The high volume fraction of the inclusion phase ($f_b = 0.3$), however, excludes the dilute scheme which is restricted to low volume concentrations (typically, $f_I < 3\%$) [50]. While the composite sphere model can accommodate such high volume fractions, the poor grading of the C-S-H$_b$ inclusion phase, which is a consequence of the (mainly mono-sized) cement particles, makes this scheme less effective for our purpose [51]. The three-phase model can accommodate both, high volume fraction and poor grading of the inclusion [52]. However, its predictive capabilities are known to become less effective when considering stiff inclusions in a compressible matrix [50], which is the case given the difference in average stiffness values of the two C-S-H phases (see Fig. 4). From these shortcomings, it appears to us that the Mori–Tanaka scheme is best suited for the given homogenization problem; and the simplicity of the scheme makes it even more attractive.

2. The second homogenization step, sketched in Fig. 7b, consists in bridging from Level I to Level II. In tohis step, the stiffness contribution of large Portlandite crystals, respectively of pores in the case of degraded materials, which take effect at an observation scale of several tens of micrometers, is homogenized over the entire microstructure REV (Level II). The characteristic length of volume V_u is $\mathcal{L}=100-150$ μm. The REV is composed of four phases: (i) large CH-Portlandite-crystals (resp. pores for degraded materials) of volume V_{CH}; (ii) the C-S-H matrix resulting from the first homogenization step of volume $V_{\text{C-S-H}}$; (iii) unhydrated cement particles (UC) of volume V_{UC}; and (iv) air voids of volume V_{V}, which are often encountered at high w/c ratios. The volume fractions of the four phases are:

$$f_{\mathrm{CH}}=\frac{V_{\mathrm{CH}}}{V_u};\quad f_{\text{C-S-H}}=\frac{V_{\text{C-S-H}}}{V_u};\quad f_{\mathrm{V}}=\frac{V_{\mathrm{V}}}{V_u};$$
$$f_{\mathrm{UC}}=\frac{V_{\mathrm{UC}}}{V_u};\quad f_{\mathrm{CH}}+f_{\text{C-S-H}}+f_{\mathrm{V}}+f_{\mathrm{UC}}=1 \tag{7}$$

From a morphological standpoint, CH, UC and air voids can be viewed as spherical inclusions in the C-S-H matrix. In fact, UC particles and CH crystals in hcp are large and of undetermined shape. Their random orientation can be effectively treated by considering a spherical inclusion morphology. It is reported that in the case of stiff inclusions embedded in a soft matrix, the exact geometry of the inclusions is of minor significance [28]. By contrast, in the case of voids exact morphological features become of primary importance. SEM images (Fig. 2) show that the new group of pores formed with the depletion of CH crystals can be well approximated with spheres. Finally, for similar reasons discussed above, the Mori–Tanaka scheme is adopted for the homogenization of the three types of spherical inclusions in a C-S-H matrix.

3.1.1. Step 1: C-S-H matrix (Level I)

The C-S-H matrix is considered a two-phase composite material, in which the stiffer C-S-H$_b$ phase plays the role of inclusion embedded in the softer C-S-H$_a$ phase considered as matrix. In the simplest case, that is in linear elastic problems, the microscopic local strains can be linked to the macroscopic strains through localization relations of the form:

$$\varepsilon_a=\mathbf{A}_a:\mathbf{E};\quad \varepsilon_b=\mathbf{A}_b:\mathbf{E} \tag{8}$$

where ε_a and ε_b represent the local strains in the two phases, related to the homogeneous (macroscopic) strain tensor $\mathbf{E}$ by 4th-order localization (or concentration) tensors $\mathbf{A}_a$ and $\mathbf{A}_b$, respectively. The macroscopic strain $\mathbf{E}$ and the macroscopic stress Σ of a representative elementary volume V_p (REV) are the volume averages of their microscopic counterparts, $\varepsilon(\mathbf{x})$ and $\sigma(\mathbf{x})$:

$$\mathbf{E}=\langle\varepsilon(\mathbf{x})\rangle_{V_p};\quad \Sigma=\langle\sigma(\mathbf{x})\rangle_{V_p} \tag{9}$$

where $\mathbf{x}$ is the position vector, and $\langle y\rangle_{V_p}=\frac{1}{V_p}\int y dV$ denotes the volume average of quantity y over domain V_p. Combining Eq. (8) with the averaging condition $(9)_1$ gives:

$$\langle\mathbf{A}\rangle_{V_p}=\mathbf{I}\Leftrightarrow f_a\mathbf{A}_a+f_b\mathbf{A}_b=\mathbf{I} \tag{10}$$

Finally, by introducing the linear elastic constitutive relations for the different phases contained in V_p, the 'effective' macroscopic stiffness tensor $\mathbf{C}$ is obtained from Eq. (8), Eq. (9) and the local phase stiffness tensors $\mathbf{c}_r$:

$$\Sigma=\langle\mathbf{c}_r:\varepsilon_r\rangle_{V_p}=\langle\mathbf{c}_r:\mathbf{A}_r\rangle_{V_p}:$$
$$\mathbf{E}\equiv\mathbf{C}:\mathbf{E}\rightarrow\mathbf{C}=\langle\mathbf{c}_r:\mathbf{A}_r\rangle_{V_p} \tag{11}$$

An estimate for the homogenized stiffness tensor follows from Eq. (11):

$$\mathbf{C}_p^{\mathrm{est}}=f_a\mathbf{c}_a:\mathbf{A}_a^{\mathrm{est}}+f_b\mathbf{c}_b:\mathbf{A}_b^{\mathrm{est}} \tag{12}$$

where $\mathbf{c}_{r=a,b}$ and $\mathbf{A}_{r=a,b}^{\mathrm{est}}$ denote, respectively, the stiffness tensor and an estimate for the localization tensor of the C-S-H$_{r=a,b}$ phases. The localization tensor $\mathbf{A}_{r=a,b}^{\mathrm{est}}$ incorporates the information about the morphology, the arrangement and the volume fractions of the phases. In the present case of a matrix-inclusion morphology, estimates of the localization tensors $\mathbf{A}_a^{\mathrm{est}}$ and $\mathbf{A}_b^{\mathrm{est}}$ are provided by the Mori–Tanaka scheme; for instance for the inclusion phase:

$$\mathbf{A}_b^{\mathrm{est}}=[\mathbf{I}+\mathbf{S}_b^{\mathrm{esh}}:(\mathbf{c}_a:\mathbf{c}_b-\mathbf{I})]^{-1}$$
$$:\langle[\mathbf{I}+\mathbf{S}_b^{\mathrm{esh}}:(\mathbf{c}_a:\mathbf{c}_b-\mathbf{I})]^{-1}\rangle_{V_p}^{-1} \tag{13}$$

where $\mathbf{S}_b^{\mathrm{esh}}$ is the Eshelby tensor of phase b. The localization tensor for the matrix phase is conveniently determined from Eq. (10):

$$\mathbf{A}_a^{\mathrm{est}}=\frac{1}{f_a}[\mathbf{I}-f_b\mathbf{A}_b^{\mathrm{est}}] \tag{14}$$

Since both phases and the homogenized material are isotropic, the stiffness tensors $\mathbf{c}_{r=a,b}$ and $\mathbf{C}_p^{\mathrm{est}}$ take the form:

$$\mathbf{c}_r=3k_r\mathbf{K}+2\mu_r\mathbf{J};\quad \mathbf{C}_p^{\mathrm{est}}=3k_p^{\mathrm{est}}\mathbf{K}+2\mu_p^{\mathrm{est}}\mathbf{J} \tag{15}$$

where $k_{r=a,b}$, $\mu_{r=a,b}$, k_p^{est} and μ_p^{est} are the bulk moduli and the shear moduli of the phases $r=a,b$ and the homogenized material; $K_{ijkl}=1/3\ \delta_{ij}\delta_{kl}$ is the volumetric part of the 4th-order unit tensor $\mathbf{I}$, and $\mathbf{J}=\mathbf{I}-\mathbf{K}$ its deviator part. The morphology of isotropic homogenized materials can be reasonably represented by phases filling up spherical inclu-

sions. The Eshelby tensor [53] for the C-S-H$_b$ phase reads as, e.g., Ref. [48],

$$\mathbf{S}_b^{\text{esh}} = \mathbf{S}_{\text{sph}}^{\text{esh}} = \alpha^{\text{est}}\mathbf{K} + \beta^{\text{est}}\mathbf{J} \tag{16}$$

with

$$\alpha^{\text{est}} = \frac{3k_a}{3k_a + 4\mu_a}; \quad \beta^{\text{est}} = \frac{6(k_a + 2\mu_a)}{5(3k_a + 4\mu_a)} \tag{17}$$

Finally, substituting Eqs. (15)–(17) into (Eqs. (12), (13) and (15) yields the homogenized bulk and shear moduli in the form:

$$k_p^{\text{est}} = k_a + \frac{f_b(k_b - k_a)}{1 + \alpha^{\text{est}} f_a\left(\frac{k_b}{k_a} - 1\right)} \tag{18}$$

$$\mu_p^{\text{est}} = \mu_a + \frac{f_b(\mu_b - \mu_a)}{1 + \beta^{\text{est}} f_a\left(\frac{\mu_b}{\mu_a} - 1\right)} \tag{19}$$

Last, the effective Young's modulus is evaluated from:

$$E_p^{\text{est}} = \frac{9k_p^{\text{est}}\mu_p^{\text{est}}}{3k_p^{\text{est}} + \mu_p^{\text{est}}} \tag{20}$$

3.1.2. Step 2: Cement paste (Level II)

Cement paste is considered as a four-phase composite material, in which the homogenized medium (C-S-H matrix) of Step 1 forms a matrix that accommodates large Portlandite crystals (CH), Voids (V), and unhydrated cement particles (UC). The following micromechanical relations hold for this homogenization step:

$$\varepsilon_{\text{C-S-H}} = \mathbf{A}_{\text{C-S-H}} : \mathbf{E}; \quad \varepsilon_{\text{CH}} = \mathbf{A}_{\text{CH}} : \mathbf{E};$$

$$\varepsilon_{\text{V}} = \mathbf{A}_{\text{V}} : \mathbf{E}; \quad \varepsilon_{\text{UC}} = \mathbf{A}_{\text{UC}} : \mathbf{E} \tag{21}$$

$$\langle \mathbf{A} \rangle_{V_u} = \sum_r f_r \langle \mathbf{A} \rangle_r = \mathbf{I} \tag{22}$$

$$\mathbf{C}_u^{\text{est}} = f_{\text{C-S-H}}\ \mathbf{c}_{\text{C-S-H}} : \mathbf{A}_{\text{C-S-H}}^{\text{est}} + f_{\text{CH}}\ \mathbf{c}_{\text{CH}} : \mathbf{A}_{\text{CH}}^{\text{est}} + f_{\text{V}}\ \mathbf{c}_{\text{V}}^{\text{est}} : \mathbf{A}_{\text{V}}^{\text{est}} : f_{\text{UC}}\ \mathbf{c}_{\text{UC}}^{\text{est}} : \mathbf{A}_{\text{UC}}^{\text{est}} \tag{23}$$

where $\mathbf{c}_{\text{C-S-H}} = \mathbf{C}_p{}^{\text{est}}$ is the stiffness tensor (Eq. (15)) from Step 1.

Given the matrix-inclusion morphology, we employ again the Mori–Tanaka scheme for estimates of the localization tensors of the inclusion phases r = CH, V, UC:

$$\mathbf{A}_r^{\text{est}} = [\mathbf{I} + \mathbf{S}_r^{\text{esh}} : (\mathbf{c}_{\text{C-S-H}}^{-1} : \mathbf{c}_r - \mathbf{I})]^{-1} : \langle [\mathbf{I} + \mathbf{S}_r^{\text{esh}} : (\mathbf{c}_{\text{C-S-H}}^{-1} : \mathbf{c}_r - \mathbf{I})]^{-1} \rangle_{V_u}^{-1} \tag{24}$$

In addition, using Eq. (22) yields the localization tensor of the matrix phase:

$$\mathbf{A}_{\text{C-S-H}}^{\text{est}} = \frac{1}{f_{\text{C-S-H}}}[\mathbf{I} - (f_{\text{CH}}\mathbf{A}_{\text{CH}}^{\text{est}} + f_{\text{V}}\mathbf{A}_{\text{V}}^{\text{est}} + f_{\text{UC}}\mathbf{A}_{\text{UC}}^{\text{est}})] \tag{25}$$

Finally, assuming isotropic elasticity, the stiffness tensors have the form:

$$\mathbf{c}_{\text{C-S-H}} = \mathbf{C}_p^{\text{est}} = 3k_p^{\text{est}}\mathbf{K} + 2\mu_p^{\text{est}}\mathbf{J};$$

$$\mathbf{c}_r = 3k_r\mathbf{K} + 2\mu_r\mathbf{J}; \quad \mathbf{C}_u^{\text{est}} = 3k_u^{\text{est}}\mathbf{K} + 2\mu_u^{\text{est}}\mathbf{J} \tag{26}$$

where k_p^{est} and μ_p^{est} are the bulk modulus and shear modulus of the C-S-H matrix, given by Eqs. (18) and (19), respectively; k_r, μ_r, k^{est} and μ^{est} are the bulk moduli and the shear moduli of the inclusion phases (r = CH, V, UC), and of the homogenized material, i.e., the cement paste.

Last, substituting Eqs. (26), (16) and (17) into Eqs. (21)–(25) yields the homogenized moduli.

3.2. Application to nondegraded and degraded cement paste

3.2.1. Input parameters: intrinsic elastic properties and volume fractions

The micromechanical model requires several input parameters for the effective elastic properties estimation: the elastic moduli k_r, μ_r and volumetric proportions f_r of each phase.

Several values for the elastic modulus of CH crystals are reported in the open literature, but values for C-S-H and clinker are scarce. Beaudoin [54] and Wittmann [55] measured the elastic modulus of CH compacts pressurized at different levels to obtain specimens with different porosities. The elastic modulus of these compacts was obtained from three-point bending tests. The intrinsic modulus of CH was found by extrapolating to zero porosity, log E vs. porosity curves. The logarithmic relation between elastic modulus and porosity shows a good fit in the range of considered porosities, however no theoretical argument supports that the assumed relationship should hold for low porosity values. Monteiro [56] used the elastic stiffness coefficients of CH, determined by the use of Brillouin Spectrum[2] in both the Voigt–Reuss bounds (V-R) and the Hashin–Strikman bounds (H-S), to obtain the following range of elastic modulus and Poisson's ratios:

$$E_{\text{CH}} = 39.77 - 44.89 \text{ GPa};$$

$$v_{\text{CH}} = 0.305 - 0.343(V - R) \tag{27}$$

[2] Measurements of the ultrasonic and hypersonic longitudinal velocities, on grown crystals and at different directions, provide the stiffness coefficients.

$$E_{CH} = 39.77 - 44.22 \text{ GPa};$$

$$v_{CH} = 0.305 - 0.325 \ (H - S) \tag{28}$$

E_{CH}, v_{CH} are the elastic modulus and Poisson's ratio of CH crystals at zero porosity. The use of nanoindentation in our experimental procedure provide a reliable means of verifying these data. Table 5 summarizes the intrinsic elastic moduli of the individual constituents found in either the open literature, or by our experiments.

It is common to determine the volumetric proportions of the different cement paste constituents by considering the hydration reactions of all cement phases from the cement composition (see Table 2). This approach, however, cannot discriminate between the two types of C-S-H. As mentioned before, a statistical analysis of the nanoindentation results provides a means of assessing the volume fractions. Alternatively, application of advanced physical chemistry models, as the one proposed by Jennings [10] and Tennis and Jennings [11], provide an estimate of these volume fractions. For the considered w/c = 0.5 cement paste, the volume fractions determined from the Jennings–Tennis model are in very good agreement with our results obtained by nanoindentation technique (C-S-H_a = 70%, C-S-H_b = 30%).

Table 5
Intrinsic elastic properties of cement paste constituents

Constituent	E (GPa)	Poissons ratio v	Method	Reference
CH	35.24		E	Beaudoin [54]
	48		E	Wittmann [55]
	$39.77 < E < 44.22$	$0.305 < v < 0.325$	B	Monteiro and Chang [56]
	36 ± 3		I	Acker [41]
	38 ± 5		I	**
Clinker				
C_3S	135 ± 7	0.3	I	Acker [41]
	147 ± 5	0.3	E	Velez et al. [57]
C_2S	140 ± 10	0.3	I	Acker [41]
	130 ± 20	0.3	E	Velez et al. [57]
C_3A	160 ± 10		I	Acker [41]
	145 ± 10		E	Velez et al. [57]
C_4AF	125 ± 25		E	Velez et al. [57]
Alite	125 ± 7		I	Velez et al. [57]
Belite	127 ± 10		I	Velez et al. [57]
C-S-H*	34 (includes both types)		E	Beaudoin and Feldman [42]
α	20 ± 2		I	Acker [41]
	21.7 ± 2.2		I	**
β	31 ± 4		I	Acker [41]
	29.4 ± 2.4		I	**
C-S-H (Leached)				
α	**3.0 ± 0.8**			**
β	**12.0 ± 1.2**	41		**

E = Extrapolation, B = Brillouin Spectrum, I = Indentation,
* The only information available for the elastic properties of C-S-H comes from nanoindentation performed at a level of 10^{-6} m.
** Experimental data from this study.
Values in bold are used in the homogenization procedure.

3.3. Nondegraded cement paste

The intrinsic elastic properties of the two types of C-S-H are:

$$E_a = 21.7 \text{ GPa}; \quad E_b = 29.4 \text{ GPa} \tag{29}$$

The Poisson's ratio for both phases is assumed to be the same, $v_a = v_b = 0.24$. Volumetric proportions, estimated using the J-T model and confirmed with nanoindentation experiments, are $f_a = 0.7$ and $f_b = 0.3$. Given these data, the elastic modulus of the C-S-H matrix is calculated using Eqs. (18)–(20):

$$E_p^{est} = E_{C\text{-}S\text{-}H} = 23.8 \text{ GPa} \tag{30}$$

Due to the high w/c ratio (>0.38), a clinker phase need not to be considered in the Level II homogenization step. The input parameters are:

- The elastic properties of the two phases, cement paste matrix and Portlandite inclusions:

$$E_{C\text{-}S\text{-}H} = 23.8 \text{ GPa}; \quad E_{CH} = 38.0 \text{ GPa};$$

$$v_{C\text{-}S\text{-}H} = 0.24; \quad v_{CH} = 0.31 \tag{31}$$

- The volumetric proportions which are estimated using the J-T model. In addition, a 3% volume fraction of air voids [41] for a w/c = 0.5 is considered; thus:

$$f_{C\text{-}S\text{-}H} = 0.86; \quad f_{CH} = 0.11; \quad f_V = 0.03 \tag{32}$$

Use of this values in the homogenization model yields:

$$E_u^{est} = 23.2 \text{ GPa} \tag{33}$$

The estimated value of the cement paste almost coincides with the experimental value $E = 22.8$ GPa obtained by UPV measurements reported in Table 4.

3.4. Degraded cement paste

The intrinsic input parameters for the calcium leached material at Level I are:

$$E_a = 3.0 \text{ GPa}; \quad E_b = 12.0 \text{ GPa};$$

$$v_{C\text{-}S\text{-}H_a} = v_{C\text{-}S\text{-}H_b} = 0.24 \tag{34}$$

The volumetric proportions of the two types were found to be not affected by calcium leaching, thus, $f_a = 0.7$ and $f_b = 0.3$. Use of this data set in Eqs. (18), (19) and (20), yields for the degraded C-S-H matrix:

$$E_p^{est} = E_{C\text{-}S\text{-}H} = 4.3 \text{ GPa} \tag{35}$$

The area previously occupied by the large CH crystals, at Level II, is now replaced by pores embedded in the

Table 6
Input–output of the two-step homogenization model for a w/c = 0.5 cement paste

Level I	Nondegraded			Degraded		
Input	E_r (GPa)	ν_r [1]	f_r [1]	E_r (GPa)	ν_r [1]	f_r [1]
C-S-H$_a$	21.7	0.24	0.7	3.0	0.24	0.7
C-S-H$_b$	29.4	0.24	0.3	12.0	0.24	0.3
Output $E_{\text{C-S-H}}$ (GPa)	23.8			4.3		

Level II	Nondegraded			Degraded		
Input	E_r [GPa]	ν_r [1]	f_r [1]	E_r [GPa]	ν_r [1]	f_r [1]
C-S-H matrix	23.8	0.24	0.86	4.3	0.24	0.86
Voids	–	–	0.03	–	–	0.14
CH	38.0	0.31	0.11	–	–	–
Output E_u^{est} (E^{exp}) (GPa)	23.2 (22.8)			3.5 (3.6)		

Given the high w/c ratio, and long hydration periods, no clinker phase is considered in the Level II homogenization.

homogenized C-S-H matrix. The volumetric proportions of the two phases are:

$$f_{\text{C-S-H}} = 0.86; \quad f_{\text{V}} = 0.14 \tag{36}$$

where the void volume fraction, f_{V}, was calculated by adding to the initial value of 3% the volume fraction of CH present in the nondegraded specimen (11%). The only input parameter is now the C-S-H matrix stiffness (Eq. (35)), and the value of the Poisson's ratio $\nu_{\text{C-S-H}} = 0.24$. This data set yields the following predicted stiffness for the calcium leached cement paste:

$$E_u^{\text{est}} = 3.5 \text{ GPa} \tag{37}$$

The value is in excellent agreement with the experimentally determined value of $E = 3.6$ GPa.

The input–output model parameters for both nondegraded and degraded cement paste are summarized in Table 6.

4. Discussion

The drop in macroscopic elasticity is a coupled consequence of (i) the increase in porosity due to dissolution of large CH crystals; and (ii) the loss of intrinsic elasticity of the C-S-H phase by decalcification. It is instructive to compare their relative importance by applying the model to two hypothetical scenarios:

- Scenario 1: Assume a cement paste with no large CH crystals (i.e., consumed in a pozzolanic reaction) subjected to calcium leaching. The predicted elastic modulus is $E_u^{\text{est}} = 4.3$ GPa, that is a residual value of 19% of the initial value of the nondegraded specimen.
- Scenario 2: The C-S-H phase is assumed to remain unaffected after leaching with only the large CH crystals being depleted. In this case, the completed degraded cement paste has an elastic modulus $E_u^{\text{est}} = 18.7$ GPa, that is 81% of its initial value.

These two scenarios demonstrate the significance of C-S-H decalcification on the overall loss of elastic stiffness, which affects four times more the chemical damage than CH crystal dissolution. The C-S-H phase dominates the volumetric proportions of cement paste materials, and its contribution to the macroscopic elastic performance is therefore significant.

5. Conclusions

1. The indentation results of two significantly different cement-based materials (our results and Acker's results [41]) suggest that the elastic properties of the two types of C-S-H are intrinsic to cement paste, originating probably from a characteristic packing during hydration. Additional tests on different types of cement paste (different w/c ratios, use of admixtures etc.) can prove/disprove this observation. By intrinsic we mean that the elastic properties of the two types of C-S-H are independent of the mix proportions, which affect only the volumetric proportions of the two types of C-S-H. Calcium leaching leads to a loss of this intrinsic elasticity, but the volume fractions of the two types of C-S-H are not affected. This suggests that calcium leaching induced aging occurs in a homogeneous way in the C-S-H matrix.

2. The experimental and theoretical results developed in this study provide evidence of the origins of the macroscopic degradation of the elastic stiffness of calcium leached cement-based material. Macroscopic measurements record residual values on the order of 16% of the initial elastic stiffness of cement paste specimens. The drop in macroscopic elasticity is a coupled consequence of (i) the increased porosity which manifests itself primarily in form of large pores present at a length scale of 10^{-5}–10^{-4} m, the space previously occupied by large CH crystals; and (ii) the loss of intrinsic elasticity of the C-S-H phase by decalcification. The decalcification of the C-S-H phase appears to be the primary source of the macroscopic elastic modulus degradation. In particular, the low density C-S-H$_a$ phase appears to be more vulnerable to chemical degradation than the dense C-S-H$_b$ phase. This suggests that a cement paste with a higher volumetric proportion of C-S-H$_b$ would be less affected by calcium-leaching-induced aging.

3. The two types of C-S-H are considered in a novel micromechanics model for cement paste that incorporates the cement paste constituents and their volumetric proportions. Combined with advanced cement chemistry models, that is here the Jennings–Tennis model which provides for a given w/c ratio the volume fractions of the two types of C-S-H, the model predicts the elastic modulus of any cement

paste with high accuracy. Since all cement paste constituents are incorporated in the model, the model equally applies to chemically degraded materials. Alternatively, the volume fractions can be determined by nanoindentation. Results obtained with this method are in very good agreement with the values provided by the J-T model.

4. The two-step homogenization model can serve as input for already existing upscaling schemes for mortars (Level III) and concrete (Level IV), e.g., [24–31]. However, in this case, the ITZ need to be added as an additional phase. Experimental results on mortar, presented in [47], underline the importance of the ITZ on the effective behavior of mortar and concrete. A three-phase model that considers the ITZ requires further information on the volumetric proportions and the elastic properties of the ITZ. Several researchers performed quantitative analysis on the ITZ [36,58,59], and several models have been proposed [60,61]. But a generalization seems still out of reach, given that the mechanical properties (and most probably the volumetric proportions of the ITZ) depend on the CH content, Ettringite, and so on, which are dissolved during calcium leaching. Further investigations on the mechanical properties and volumetric proportions of the ITZ are necessary to properly predict the loss of elastic stiffness of mortar and concrete subjected to leaching.

Acknowledgements

This research was performed as part of Grant No. DE-FG03-99SF21891/A000 of the U.S. Department of Energy (DOE) to MIT. The authors gratefully acknowledge the support of this work by the Nuclear Energy Research Initiative Program of DOE, and the collaboration with the Commissariat à l'Energie Atomique (C.E.A., Saclay, France), through Dr. Jérôme Sercombe. The authors also thank Prof. Shi-Chang Wooh, Prof. Lorna Gibson, Prof. Subra Suresh and Dr. Neal S. Berke of W.R. Grace for providing the equipment for the experimental program of this study; and Dr. Eric Lemarchand for useful advice on the use of micromechanical models. The authors would also like to thank Krystyn van Vliet for the execution of nanoindentation tests. Partial financial support from the CEE department of MIT to the first author under the Rosenblith and Presidential fellowship is also gratefully acknowledged.

References

[1] J. Taplin, A method for following the hydration reaction in Portland cement paste, Aust. J. Appl. Sci. 10 (1959) 329–345.
[2] B. Dalgleish, K. Ibe. Thin foil studies of hydrated cements, Cem. Concr. Res. 11 (5) (1981) 729–740.
[3] G. Groves, TEM studies of cement hydration, Mater. Res. Soc. Symp. Proc. 85 (1987) 3–12.
[4] I. Richardson, S. Rodger, G. Groves, The porosity and pore structure of hydrated cement pastes as revealed by electron microscopy techniques, Mater. Res. Soc. Symp. Proc. 137 (1989) 313–318.
[5] D. Viehland, J. Li, L. Yuan, Z. Xu, Mesostructure of calcium silicate hydrate (C-S-H) gels in Portland-cement paste—A short range ordering, nanocrystallinity and local compositional order, J. Am. Ceram. Soc. 79 (7) (1996) 1731–1744.
[6] I. Richardson, The nature of C-S-H in hardened cements, Cem. Concr. Res. 29 (8) (1999) 1131–1147.
[7] H. Taylor, Studies on the chemistry and microstructure of cement pastes, Proc. Br. Ceram. Soc. 35 (1984) 65–82.
[8] H. Taylor, D. Newbury, An electron microprobe study of a mature cement paste, Cem. Concr. Res. 14 (4) (1984) 565–573.
[9] J. Thomas, H. Jennings, A. Allen, The surface area of cement paste as measured by neutron scattering: Evidence for two C-S-H morphologies, Cem. Concr. Res. 28 (6) (1998) 897–905.
[10] H.M. Jennings, A model for the microstructure of calcium silicate hydrate in cement paste, Cem. Concr. Res. 30 (1) (2000) 101–116.
[11] P.D. Tennis, H.M. Jennings, A model for two types of calcium silicate hydrate in the microstructure of Portland cement pastes, Cem. Concr. Res. 30 (6) (2000) 855–863.
[12] S. Diamond, D. Bonen, Microstructure of hardened cement paste—A new interpretation, J. Am. Ceram. Soc. 76 (12) (1993) 2993–2999.
[13] K. Scrivener, H. Patell, P. Pratt, L. Parrott, Analysis of phases in cement paste using backscattered electron images, methanol adsorption and thermogravimetric analysis, Mater. Res. Soc. Symp. Proc. 85 (1985) 67–76.
[14] H. Taylor, Cement Chemistry, 2nd ed., Thomas Telford, London, 1997.
[15] F. Adenot, Durabilité du béton: Caractérisation et Modélisation des Processus Physiques et Chimiques de Dégradation du Ciment, PhD Dissertation, University of Orleans, France (1992) (in French).
[16] C. Carde, R. Francois, J. Torrenti, Leaching of both calcium hydroxide and C-S-H from cement paste: Modeling the mechanical behavior, Cem. Concr. Res. 26 (8) (1996) 1257–1268.
[17] C. Carde, Caractérisation et Modélisation de l'altération des Proprietés Mécaniques Due a la Lixiviation des Matériaux Cimentaires, PhD Dissertation, INSA Toulouse, France (1996) (in French).
[18] C. Carde, R. Francois, Effect of the leaching of calcium hydroxide from cement paste on mechanical and physical properties, Cem. Concr. Res. 27 (4) (1997) 539–550.
[19] F. Heukamp, F.-J. Ulm, J. Germaine, Mechanical properties of calcium leached cement pastes: Triaxial stress states and the influence of the pore pressure, Cem. Concr. Res. 31 (5) (2001) 767–774.
[20] F. Heukamp, F.-J. Ulm, J. Germaine, Poroplastic properties of calcium leached cement-based materials, Cem. Concr. Res., Submitted for publication.
[21] F.-J. Ulm, J.-M. Torrenti, F. Adenot, Chemoporoplasticity of calcium leaching in concrete, ASCE J. Eng. Mech. (1999) 1200–1211.
[22] F.-J. Ulm, F. Heukamp, Monitoring the durability performance of concrete in nuclear waste containment, Annual report, Department of Energy (2000).
[23] B. Gérard, Contribution des couplages mécanique-chimie-transfert dans la tenue à long terme des ouvrages de stockage des déchets radioactifs, PhD Dissertation, ENS Cachan, France (1996) (in French).
[24] G.Q. Li, Y. Zhao, S.S. Pang, Y.Q. Li, Effective Young's modulus estimation of concrete, Cem. Concr. Res. 29 (9) (1999) 1455–1462.
[25] G.Q. Li, Y. Zhao, S.S. Pang, Four-phase sphere modeling of effective bulk modulus of concrete, Cem. Concr. Res. 29 (6) (1999) 839–845.
[26] E.J. Garboczi, J.G. Berryman, Elastic moduli of a material containing composite inclusions: Effective medium theory and finite element computations, Mech. Mater. 33 (8) (2001) 455–470.
[27] E.J. Garboczi, D.P. Bentz, Digital-simulation of the aggregate–cement paste interfacial zone in concrete, J. Mater. Res. 6 (1) (1991) 196–201.
[28] P. Simeonov, S. Ahmad, Effect of transition zone on the elastic behavior of cement-based composites, Cem. Concr. Res. 25 (1) (1995) 165–176.
[29] C.C. Yang, R. Huang, Double inclusion model for approximate elastic moduli of concrete material, Cem. Concr. Res. 26 (1) (1996) 83–91.

[30] C.C. Yang, Effect of the transition zone on the elastic moduli of mortar, Cem. Concr. Res. 28 (5) (1998) 727–736.
[31] G. Ramesh, E.D. Sotelino, W.F. Chen, Effect of transition zone on elastic moduli of concrete materials, Cem. Concr. Res. 26 (4) (1996) 611–622.
[32] P. Stutzman, J. Clifton, Specimen preparation for scanning electron microscopy, in: L. Jany, A. Nisperos (Eds.), Proceedings of the Twenty-First International Conference on Cement Microscopy, International Cement Microscopy Association, Duncanville, Las Vegas, NV, 1999, pp. 10–22.
[33] P. Faucon, A. Delagrave, J. Petit, C. Richet, J. Marchand, H. Zanni, Aluminum incorporation in calcium silicate hydrate (C-S-H) depending on their Ca/Si ratio, J. Phys. Chem., B 103 (1999) 7796–7802.
[34] C. Porteneuve, H. Zanni, C. Vernet, K. Kjellsen, J.-P. Korb, D. Petit, Nuclear magnetic resonance characterization of high- and ultrahigh-performance concrete: Application to the study of water leaching, Cem. Concr. Res. 31 (12) (2001) 1887–1894.
[35] T.A. Venkatesh, K.J. van Vliet, A.E. Giannakopoulos, S. Suresh, Determination of elasto-plastic properties by instrumented sharp indentation: Guidelines for property extraction, Scr. Mater. 42 (9) (2000) 833–839.
[36] W.Z. Zhu, P.J.M. Bartos, Application of depth-sensing microindentation testing to study of interfacial transition zone in reinforced concrete, Cem. Concr. Res. 30 (8) (2000) 1299–1304.
[37] W.C. Oliver, G.M. Pharr, An improved technique for determining hardness and elastic-modulus using load and displacement sensing indentation experiments, J. Mater. Res. 7 (6) (1992) 1564–1583.
[38] M.F. Doerner, W.D. Nix, A method for interpreting the data from depth sensing indentation instruments, J. Mater. Res. 1 (1986) 601–609.
[39] A. Giannakopoulos, S. Suresh, Determination of elastoplastic properties by instrumented sharp indentation, Scr. Mater. 40 (10) (1999) 1191–1198.
[40] A.E. Giannakopoulos, P.L. Larsson, R. Vestergaard, Analysis of vickers indentation, Int. J. Solids Struct. 31 (19) (1994) 2679–2708.
[41] P. Acker, Micromechanical analysis of creep and shrinkage mechanisms, in: F.-J. Ulm, Z. Bazant, F. Wittmann (Eds.), Creep, Shrinkage and Durability Mechanics of Concrete and other Quasi-Brittle Materials, Elsevier, Oxford, UK, 2001.
[42] J. Beaudoin, R. Feldman, Dependence of degree of silica polymerization and intrinsic mechanical properties of C-S-H on C/S, 8th International Congress on the Chemistry of Cement, Rio de Janeiro, 1986.
[43] ASTM C 597-83, Standard test method for pulse velocity through concrete.
[44] H.F.W. Taylor, BS 1881: Part 203, Ultrasonic Pulse Velocity meauserements, BS.
[45] V. Malhotra, Testing Hardened Concrete: Nondestructive Methods, American Concrete Institute: Monograph no. 9, Iowa State University Press, Ames, IA, 1976.
[46] C.L. Bellégo, Couplages chimie-mécanique dans les structures en béton attaquées par l'eau: Étude expérimentale et analyse numérique, PhD Dissertation, ENS Cachan, France (2001) (in French).
[47] G. Constantinides, F.-J. Ulm, The elastic properties of calcium-leached cement pastes and mortars: A multi-scale investigation, MIT CEE Report R02–01.
[48] A. Zaoui, Materiaux heterogenes et composites, lecture notes, Ecole Polytechnique, Paris (1997) (in French).
[49] T. Mori, K. Tanaka, Average stress in matrix and average elastic energy of materials with misfitting inclusions, Acta Metall. 21 (5) (1973) 571–574.
[50] R. Christensen, A critical evaluation for a class of micromechanics models, J. mech. phys. solids 38 (3) (1990) 379–404.
[51] Z. Hashin, The elastic moduli of heterogenous material, J. Appl. Mech. Transactions of the ASME 29 (1962) 143–150.
[52] Z. Hashin, Analysis of composite-materials—A survey, J. Appl. Mech. Transactions of the ASME 50 (3) (1983) 481–505.
[53] J.D. Eshelby, The determination of the elastic field of an ellipsoidal inclusion, Proc. R. Soc. Lond. A 241 (1957) 376–392.
[54] J. Beaudoin, Comparison of mechanical properties of compacted calcium hydroxide and portland cement paste systems, Cem. Concr. Res. 13 (3) (1983) 319–324.
[55] F.H. Wittmann, Estimation of the modulus of elasticity of calcium hydroxide, Cem. Concr. Res. 16 (6) (1986) 971–972.
[56] P.J.M. Monteiro, C.T. Chang, The elastic-moduli of calcium hydroxide, Cem. Concr. Res. 25 (8) (1995) 1605–1609.
[57] K. Velez, S. Maximilien, D. Damidot, G. Fantozzi, F. Sorrentino, Determination by nanoindentation of elastic modulus and hardness of pure constituents of Portland cement clinker, Cem. Concr. Res. 31 (4) (2001) 555–561.
[58] W. Zhu, P.J.M. Bartos, Assessment of interfacial microstructure and bond properties in aged GRC using a novel microindentation method, Cem. Concr. Res. 27 (11) (1997) 1701–1711.
[59] I. Odler, A. Zurz, Structure and bond strength of cement aggregates interfaces, in: S. Mindess (Ed.), Bonding in Cementitious Materials, Symposium Proceedings, vol. 114, Materials Research Society, MRS, Pittsburg, PA, 1988, pp. 21–27.
[60] E. Garboczi, D. Bentz, Analytical formulas of interfacial transition zone properties, Adv. Cem. Based Mater. 6 (1997) 99–108.
[61] M.P. Lutz, P.J.M. Monteiro, R.W. Zimmerman, Inhomogeneous interfacial transition zone model for the bulk modulus of mortar, Cem. Concr. Res. 27 (7) (1997) 1113–1122.